Supramolecular motifs in metal complexes of Schiff bases. Part 5.[1] Zinc(II)-assisted self-assembly of some bis-*N*,*N*- and *N*,*O*-bidentate Schiff bases and chiral packing modes in solid state

Noboru Yoshida,*[a] Kazuhiko Ichikawa[a] and Motoo Shiro[b]

[a] *Laboratory of Molecular Functional Chemistry, Division of Material Science, Graduate School of Environmental Earth Science, Hokkaido University, Sapporo 060-0810, Japan*
[b] *Rigaku Corporation, Akishima, Tokyo 196-8666, Japan*

Received (in Cambridge, UK) 6th October 1999, Accepted 26th October 1999

Zinc(II)-assisted self-assembly of a new bis-*N*,*O*-bidentate Schiff base ligand, (*N*-salicylidene-4,4′-diaminodiphenyl)-methane (L^{16}) with two chelating sites linked by a spacer group (-$C_6H_4CH_2C_6H_4$-), afforded in high yield the double-helical dinuclear complex (L^{16} : Zn^{II} = 2 : 2). Single-crystal X-ray analyses demonstrated clearly that the two Zn^{II} centers have a distorted tetrahedral (T_d) coordination sphere with two-wrapped ligands. The analogous Schiff base, bis[4-(2-pyridylmethyleneaminophenyl]methane (L^{17}) was also designed to self-assemble in the presence of metal ions, leading to a triple-helical dinuclear (L^{17} : Zn^{II} = 3 : 2) supramolecular motif. Each zinc ion has six-coordinate octahedral geometry with six nitrogens from three ligands. These unprecedented helical motifs in the solid state and solution seem to be induced by the geometrical preference for octahedral or tetrahedral coordination mode of the Zn^{II} ion and the interligand π-stacking interactions between the spacer groups of L^{16} and L^{17}. Electrospray mass spectrometry proved a very useful characterisational tool in detecting the distribution of supramolecular species in solution. Use of a *N*,*N*′-bis(2-pyridylmethylene)-1,4-diaminobenzene (L^{35}) with a rigid phenylene spacer in its center resulted in the one-dimensional zigzag polymeric structure ((L^{35} : Zn^{II})$_\infty$ = (1 : 1)$_\infty$) where the multiple π-stacking interactions operate between the aromatic rings of linking ligands. Each zinc ion is octahedrally coordinated by two *N*,*N*-bidentate arms of two different ligands and two *cis* oxygens from *N*,*N*-dimethylformamide as coordinating solvent.

Introduction

Recent synthetic advances using Schiff base ligands[1–5] with aromatic spacer groups and other flexible bis-bidentate ligands[6–15] as building blocks for metal-assisted self-assembly (metallosupramolecular chemistry) have demonstrated the requirements for the close and tunable control of the coordination sphere of the metal ion and the weak aromatic interactions between the spacer groups in the ligand. The mechanism and structure for the formation of metal-assisted self-assembled complexes are often impossible to predict in advance and many subtle factors such as π–π interactions,[2,16] templated-anions,[17–19] trapped-cations,[20] deprotonation of the site remote from the metal center[7b,21] and the preferred coordination geometry of metal ion[22] can influence the final product.

Achiral bridged Schiff bases, the previously designed series of bis-bidentate ligands shown in Scheme 1, have been shown to spontaneously wrap around copper(II) ion to create a self-assembled helical multinuclear complex in the solid state.[1] Formation of some helical multinuclear supramolecular motifs has been explained on the basis of self-assembly processes involving π stacking of the spacer group (X) with free rotational freedom and a flexible coordination mode for tetrahedral and square-planar geometries of the Cu^{II} ion.

Zinc(II) ion has been widely found in several zinc-containing metalloenzymes such as zinc-peptidases,[23] human carbonic anhydrase,[24] and alkalinephosphatase.[25] The coordination mode for octahedral or tetrahedral geometries of zinc(II) ion may affect the formation and mechanism of the self-assembly processes of bis-bidentate Schiff bases. Furthermore, the CH···π interactions, which have recently received much attention in supramolecular architectures, have also been important in a variety of molecular phenomena at physical, chemical, and biological levels.[26] We report here a one-pot self-assembly synthesis of several zinc(II) complexes utilizing weak CH···π and π···π interactions of a novel type of Schiff base ligand, L^{16}, L^{17}, and L^{35} as shown in Scheme 2. The variations in (a) metal-binding site from pyridylmethylene *N*,*N* moiety to

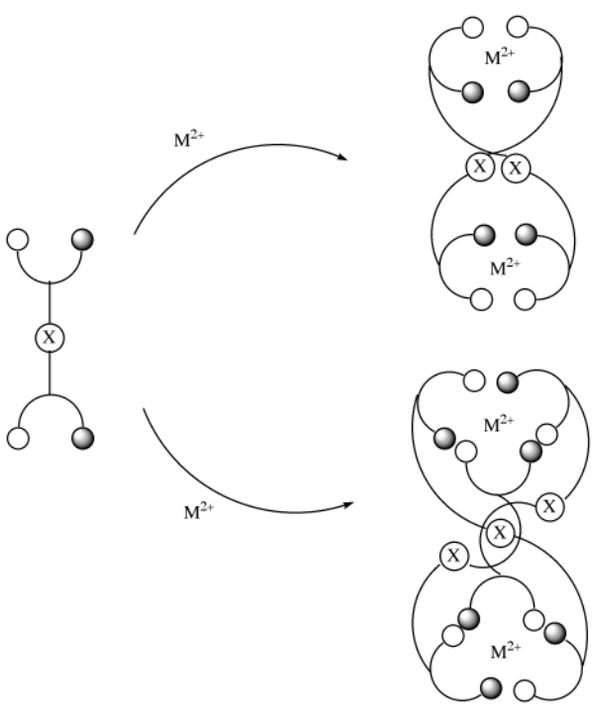

Scheme 1

Table 1 Crystallographic data, data collection and refinement parameters for **1**·DMF·2CH_3CN, **2**·2$CHCl_3$, and **3**·3DMF

	1·DMF·2CH_3CN	**2**·2$CHCl_3$	**3**·3DMF
Formula	$C_{82}H_{73}N_{15}O_{17}Cl_4Zn_2$	$C_{56}H_{42}N_4O_4Cl_6Zn_2$	$C_{27}H_{35}N_7O_{11}Cl_2Zn$
M	1813.14	1178.45	769.90
Crystal system	Monoclinic	Monoclinic	Monoclinic
Space group	*C*2/*c* (no. 15)	$P2_1/c$ (no. 14)	$P2_2/a$ (no. 14)
Unit cell dimensions			
a/Å	54.89(2)	18.263(4)	13.472(2)
b/Å	13.833(2)	16.089(3)	18.812(3)
c/Å	22.01(1)	19.160(4)	14.538(4)
β/°	95.40(3)	109.22(3)	106.17(1)
U/Å^3	16639.9	5316(2)	3539(2)
Z	8	4	4
T/K	298(2)	298(1)	173(1)
μ(Mo-Kα)/cm^{-1}	7.82	12.54	9.09
No. of reflections measured	10268	7883	5297
Residuals: *R*,[a] *Rw*[b]	0.061, 0.084	0.077, 0.095	0.052, 0.075

[a] $R = \Sigma ||F_o| - |F_c||/\Sigma|F_o|$. [b] $Rw = [\Sigma\omega(|F_o| - |F_c|)^2/\Sigma\omega|F_o|^2]^{1/2}$, $\omega = 1/\sigma^2(F_o) = [\sigma^2(F_o) + p^2(F_o)^2/4]^{-1}$.

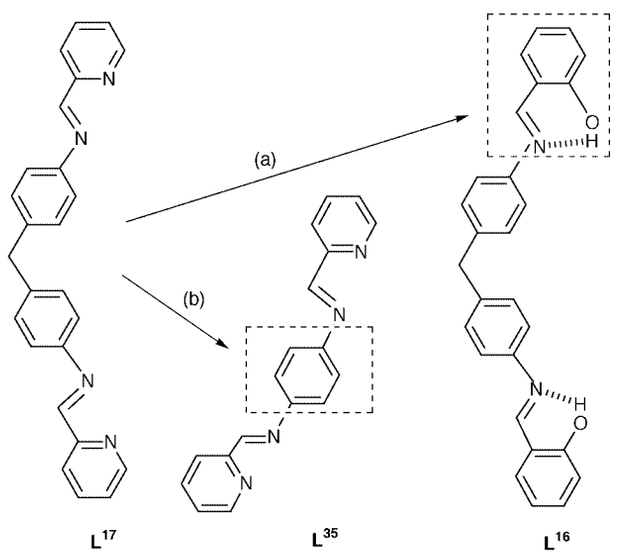

Scheme 2 (a) Change in the coordination site from *N*,*N* bidentate to *N*,*O* bidentate. (b) Change into the shorter spacer group.

salicylidene *O*,*N* one ($L^{17}\rightarrow L^{16}$) and (b) spacer group from diphenylmethylene -$C_6H_4CH_2C_6H_4$- to phenylene -C_6H_4- ($L^{17}\rightarrow L^{35}$) may produce some zinc(II) complexes with unprecedented supramolecular motifs.

Experimental

Preparation of Schiff base ligands, L^{17}, L^{16}, and L^{35}, and their Zn^{II} complexes

Ligand L^{17} was synthesized by usual Schiff-base condensation of bis(4-aminophenyl)methane and pyridine-2-aldehyde.[2] To a stirred solution of bis(4-aminophenyl)methane (6.09 g, 0.0307 mol) in ethanol (300 ml) at room temperature was added dropwise an ethanolic solution of pyridine-2-aldehyde (6.58 g, 0.0615 mol). After the addition was complete, the reaction mixture was heated to 70–80 °C. The resultant precipitate was filtered off, washed with ethanol, and dried in air to afford 9.0 g (78%) of pale-yellow crystalline product. Calcd. for $C_{25}H_{20}N_4$: C, 79.76; H, 5.35; N, 14.88; found: C, 79.59; H, 5.43; N, 14.93%. ^{1}H-NMR (400 MHz, DMF-d_7 (99.5%), 25 °C, internal ref. TMS): δ 8.74 (2H, ddd, *J* = 4.9, 2.0, 0.9, pyridyl H^6), 8.65 (2H, s, -CH=N-), 8.21 (2H, ddd, *J* = 7.8, 2.0, 1.0, pyridyl H^3), 7.98 (2H, td, *J* = 7.8, 1.5, pyridyl H^4), 7.54 (2H, ddd, *J* = 7.5, 5.0, 1.4, pyridyl H^5), 7.36 and 7.40 (8H, dd, *J* = 7.8, 1.5, aminophenyl), 4.09 (2H, s, -CH_2-).

Ligand L^{16} was synthesized in 90% yield by heating ethanolic solutions containing bis(4-aminophenyl)methane (1 equiv.) and salicylaldehyde (2 equiv.). Data for ligand L^{16}: fluorescent yellow powder, 90% yield (Calcd. for $C_{27}H_{22}N_2O_2$; C, 79.78; H, 5.45; N, 6.89. Found: C, 79.78; H, 5.65; N, 6.89%). ^{1}H-NMR (400 MHz, $CDCl_3$, 25 °C, internal ref. TMS): δ 13.29 (2H, ddd, OH···H), 8.62 (2H, s, -CH=N-), 7.38 (2H, d, *J* = 7.3, sal-ad H^6), 7.37 (2H, td, sal-ad H^4), 7.27 and 7.23 (8H, ddd, bis-(amino)phenyl), 7.02 (2H, d, *J* = 7.8, sal-ad H^3), 6.94 (2H, td, *J* = 7.8, 1.0, sal-ad H^5), 4.04 (2H, s, -CH_2-).

Ligand L^{35} was synthesized by the same condensation of 1,4-phenylenediamine and pyridine-2-aldehyde and obtained as dark orange crystals, yield 70% (Calcd. for $C_{18}H_{14}N_4$: C, 75.5; H, 4.92; N, 19.56. Found: C, 75.36; H, 5.06; N, 19.25%). ^{1}H-NMR (400 MHz, $CDCl_3$, 30 °C, internal ref. TMS): δ 8.73 (2H, ddd, *J* = 4.9, 1.5, 1.0, pyridyl H^6), 8.67 (2H, s, -CH=N-), 8.22 (2H, ddd, *J* = 7.8, 1.3, 1.0, pyridyl H^3), 7.83 (2H, td, *J* = 7.3, 1.5, pyridyl H^4), 7.38 (2H, ddd (overlapped with diaminobenzene), pyridyl H^5), 7.38 (4H, s, diaminobenzene).

Synthesis and characterization of the zinc(II) complexes of L^{17} and L^{16} used in this study were carried out by the usual synthetic method.[2,3] For example, a mixture of L^{17} (0.64 g, 1.7 mmol) and $Zn(ClO_4)_2$·$6H_2O$ (0.33 g, 1.7 mmol) in CH_3OH (50 ml) was stirred at room temperature for several hours. The resultant pale-yellow precipitate was filtered off and air-dried. The yields of this material were *ca.* 50–60%, but were not optimised. Pale-yellow crystals were obtained by slow diffusion of diethyl ether in the DMF–MeCN solution (Found: C, 53.62; H, 3.97; N, 10.50; Cl, 7.84%. Calcd. for $C_{75}H_{60}N_{12}O_{16}Cl_4Zn_2$·DMF·2MeCN: C, 54.32; H, 4.05; N, 11.58; Cl, 7.82%).

Reaction of L^{16} (3 equiv.) with $Zn(ClO_4)_2$·$6H_2O$ (2 equiv.) and K_2CO_3 (2 equiv.) in methanol at room temperature affords a fluorescent yellow solid (Found: C, 53.69; H, 4.05; N, 4.62%. Calcd. for $C_{54}H_{50}N_4O_{16}Cl_2Zn_2$: C, 53.48; H, 4.15; N, 4.62%) which is soluble in $CHCl_3$. Fluorescent-yellow crystals were obtained by slow diffusion of diethyl ether into the $CHCl_3$ solution of the metal complex.

Reaction of a methanol solution of 1 equiv. of the ligand L^{35} with $Zn(ClO_4)_2$·$6H_2O$ (1 equiv.) at room temperature leads to the deep orange solids with L^{35}:Zn^{II} = 2:2 and 3:2 ratio as judged by elemental analysis. The yield was in the range 60–70%. (Calcd. for$C_{54}H_{42}N_{12}O_{16}Cl_4Zn_2$ as 3:2 complex: C, 46.74; H, 3.05; N, 12.11; Cl, 10.22 and $C_{36}H_{28}N_8O_{16}Cl_4Zn_2$ as 2:2 complex: C, 39.26; H, 2.56; N, 10.17; Cl, 12.87. Found: C, 42.48; H, 3.40; N, 11.04; Cl, 10.07%). X-Ray quality crystals were grown by slow diffusion of diethyl ether into a DMF solution of the crude material.

Single crystal X-ray structure analysis

Single crystals suitable for X-ray analysis of **1** ($[Zn_2(L^{17})_3](ClO_4)_2$), **2** ($[Zn_2(L^{16} - 2H)_2]$) and **3** ($[Zn^{II}L^{35}]$·$(ClO_4)_2$) were obtained from DMF–MeCN/ether, $CHCl_3$/ether, and DMF/

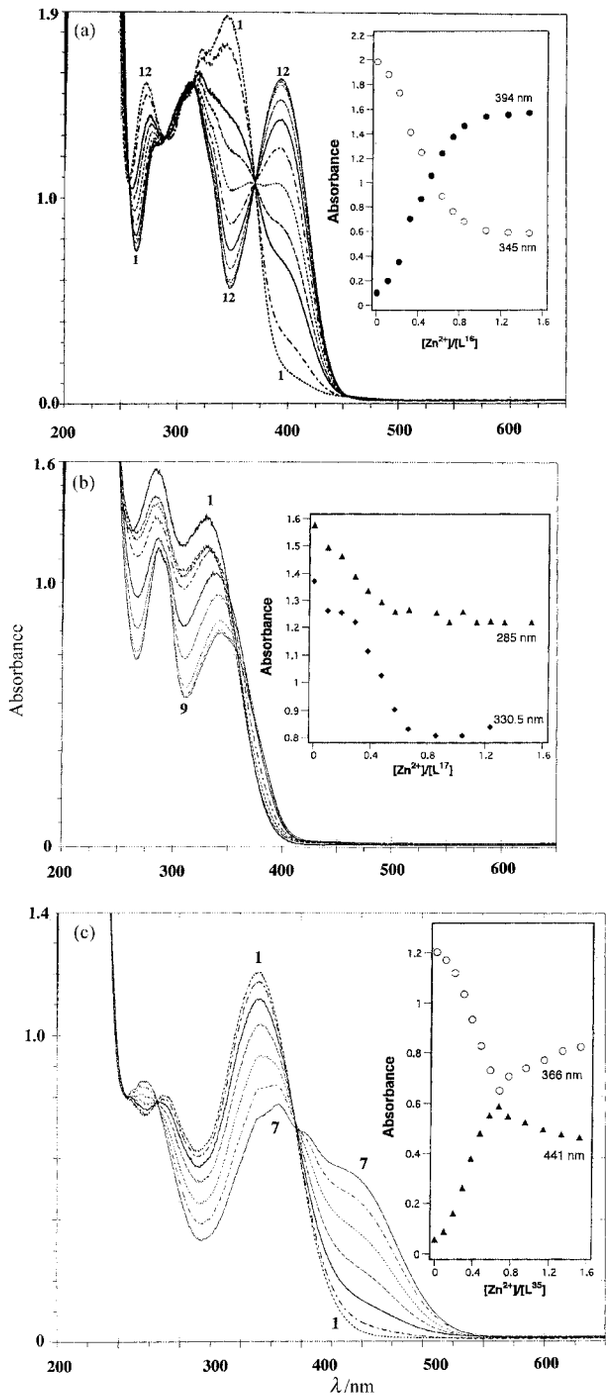

Fig. 1 UV/VIS spectral changes of ligands L^{16} (a), L^{17} (b) and L^{35} (c) in ethanol upon addition of $Zn(CH_3COO)_2{\cdot}2H_2O$. $[L^{16}] = [L^{17}] = [L^{35}] = 6.50 \times 10^{-5}$ mol dm^{-3}.

ether, respectively. Precise data collection and crystal parameters for **1**, **2** and **3** are summarized in Table 1. CCDC reference number 188/193. The structure was solved by direct method[27] and expanded using Fourier techniques.[28] The non-hydrogen atoms were refined anisotropically. Hydrogen atoms were included but not refined. All calculations were performed using the teXsan[29] crystallographic software package of Molecular Structure Coorporation.

Results and discussion

UV/VIS titrations in the formation of Zn^{II} complexes with L^{16}, L^{17}, and L^{35}

The UV/VIS spectrum for L^{16} is quite sensitive to the acidity of the solution and the presence of Cu^{II} ion. Fig. 1(a) represents the change in the UV/VIS spectrum of L^{16} upon addition of Zn^{II} ion in ethanol. Four isosbestic points are observed at $\lambda = 289$, 314.5, 370, and 454 nm. Upon increasing Zn^{II} concentration, there is a decrease in absorbance of the ligand π–π^* (CH=N) band at 345 nm and emergence of a new peak at 394 nm due to deprotonation of the phenol group and the Zn^{II} coordination. A molar ratio plot at 345 and 394 nm demonstrates the formation of a $Zn^{II}:L^{16} = 1:1$ ratio complex, as judged by the clear inflection at $[Zn^{II}]/[L^{16}] = 1$.

A smaller UV/VIS change (Fig. 1(b)) is observed in the case of the L^{17}–Zn^{2+} system and an isosbestic point is not observed under similar conditions. An inflection at $[Zn^{II}]/[L^{17}] = ca.\ 0.66$ ($\lambda_{obs} = 330.5$ nm) may suggest the formation of $Zn^{II}:L^{17} = 2:3$ complex. UV/VIS titration (Fig. 1(c)) was performed also in the L^{35}/Zn^{2+} system. Since L^{35} has a considerably delocalized π-conjugate system, the π–π^* band due to the coordination of the Zn^{II} ion shows a large red shift up to 450 nm. The magnitude of this red-shift on coordination is approximately 100 nm, suggesting that the induced π-conjugation in the five-membered chelate rings occurs effectively through the spacer in the L^{35}–Zn^{2+} system. The result is a deepening in colour from colourless to orange–yellow. Some isosbestic points at 281.5 and 395 nm and a molar ratio plot suggest the formation of $Zn^{II}:L^{35} = 2:3$ complex. It is interesting to note that the UV/VIS absorption change at higher Zn^{II} concentration of $[Zn^{II}]/[L^{35}] > ca.\ 0.6$ reverses both at $\lambda = 366$ and 441 nm.

Mass spectra of Zn^{II} complexes with L^{16}, L^{17}, and L^{35} complexes

Positive electrospray ionization mass spectrometry (ESI-MS) of the L^{16}–Zn^{II} complex in MeOH (trace $CHCl_3$) shows the presence of several aggregated species (Fig. 2). The fairly weak peak at $m/z = 1879.1$ could be assignable to the tetranuclear mono-protonated species, $[Zn_4(L^{16} - 2H)_4]H^+$, $(4:4)^+$. Two peaks corresponding to the binuclear mono-protonated $[Zn_2(L^{16} - 2H)_2]H^+$, $(2:2)^+$ species and trinuclear mono-protonated $[Zn_3(L^{16} - 2H)_3]H^+$, $(3:3)^+$ species are strongly observed at $m/z = 941.0$ and 1408.9, respectively. The experimental isotope profiles were in excellent agreement with the theoretical isotope distributions expected for the $[Zn_3(L^{16} - 2H)_3]H^+$.

The solution behaviour of the L^{17}–Zn^{II} complex was analyzed by two types of mass spectrometry, ESI-MS and fast atom bombardment mass spectrometry (FAB-MS). FAB-MS of the L^{17}–Zn^{II} complex is very complicated but informative on the successive loss of ClO_4^- or $HClO_4$ from neutral species, **1** ($[Zn_2(L^{17})_3](ClO_4)_2$) (Fig. 3). The FAB-MS (3-nitrobenzyl alcohol as a matrix in DMF as solvent) shown in Fig. 3 displays several characteristic peaks for $(Zn^{II}:L^{17})^{n+} = (1:1)^+$, $(1:2)^+$, $(2:2)^+$, and $(2:3)^+$ species (minus ClO_4^- or $HClO_4$), where $M_{1:1}$, $M_{1:2}$, $M_{2:2}$, and $M_{2:3}$ denote the species $[ZnL^{17}](ClO_4)_2$, $[Zn(L^{17})_2](ClO_4)_2$, $[Zn_2(L^{17})_2](ClO_4)_4$, and $[Zn_2(L^{17})_3](ClO_4)_4$, respectively. The peaks for higher aggregates $[M_{2:3} - ClO_4 - (HClO_4)_2]^+$, $[M_{2:3} - ClO_4 - HClO_4]^+$, and $[M_{2:3} - ClO_4]^+$ can be detected at $m/z = 1358.0$, 1458.0, and 1559.0, respectively.

ESI-MS of the L^{17}–Zn^{II} complex in MeOH is significantly different from the FAB-MS observed in the same complex (Fig. 4). The most important peak corresponding to the dinuclear-triple motif of crystal structure **1** (*vide infra*) is $[M_{2:3} - ClO_4]^+$ at $m/z = 1558.6$. It is noted that minor 1:1 complexes that are solvated by several MeOH molecules ($[M_{1:1}(MeOH)_2 - ClO_4]^+$ and $[M_{1:1}(MeOH)_3 - ClO_4]^+$) are clearly detected at $m/z = 606.0$ and 636.1.

Fig. 5 shows the ESI-MS of the L^{35}–Zn^{II} complex in methanol. The peaks at $m/z = 349.2$, 451.2, and 637.5 could be assigned to lower aggregates $[M_{1:1} - ClO_4 - HClO_4]^+$, $[M_{1:1} - ClO_4]^+$, and $[M_{1:2} - ClO_4 - HClO_4]^+$. Higher aggregates such as $Zn^{II}:L^{35} = 2:2$ and 2:3 complexes are not observed in this system.

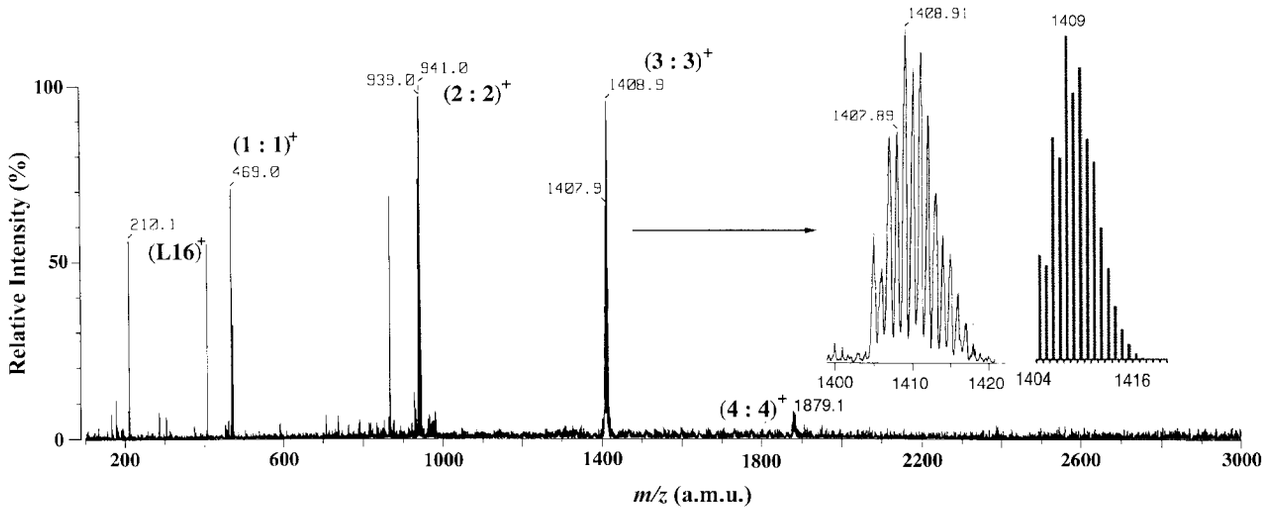

Fig. 2 ESI mass spectrum of a methanol solution of **2**.

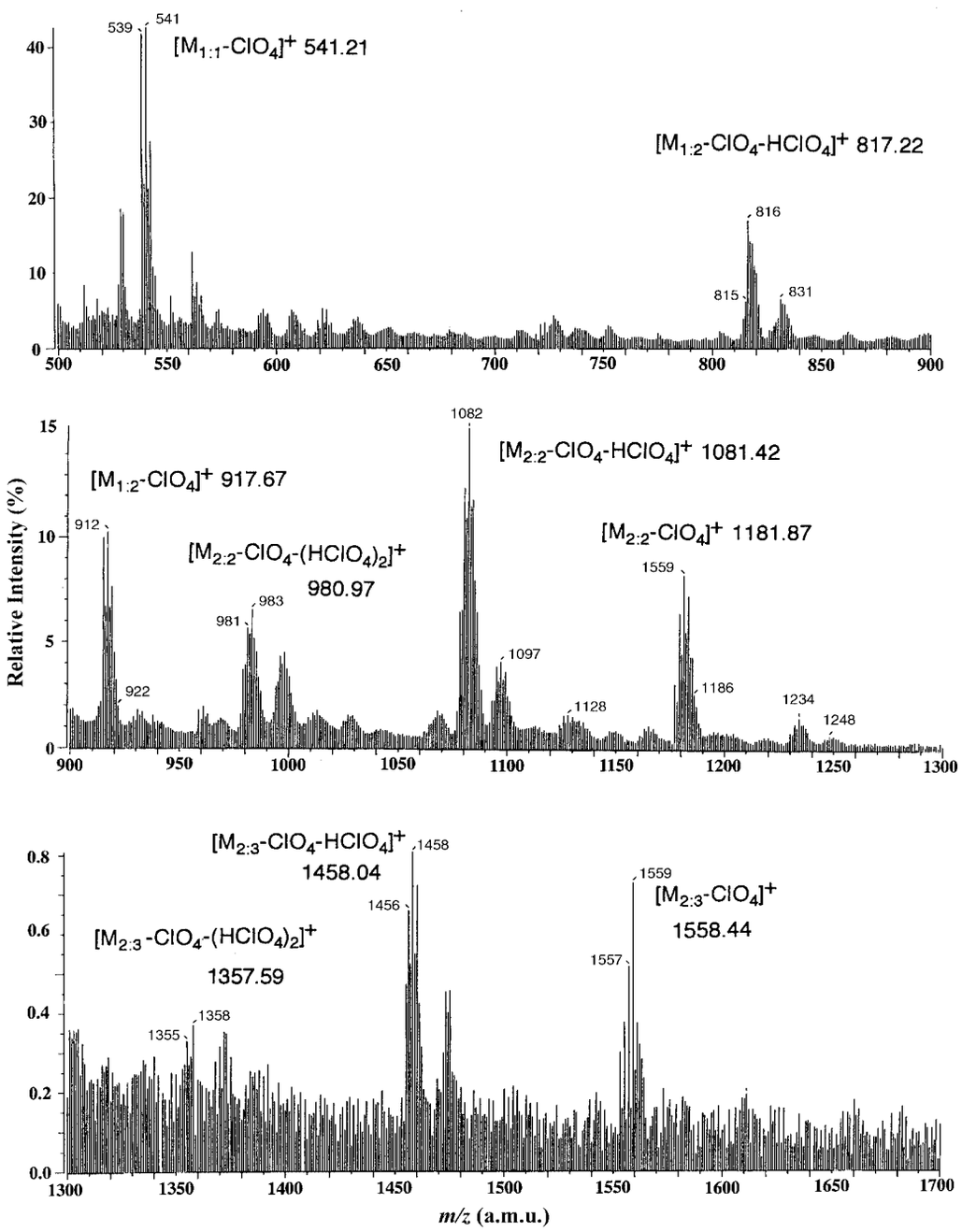

Fig. 3 FAB mass spectrum for **1**.

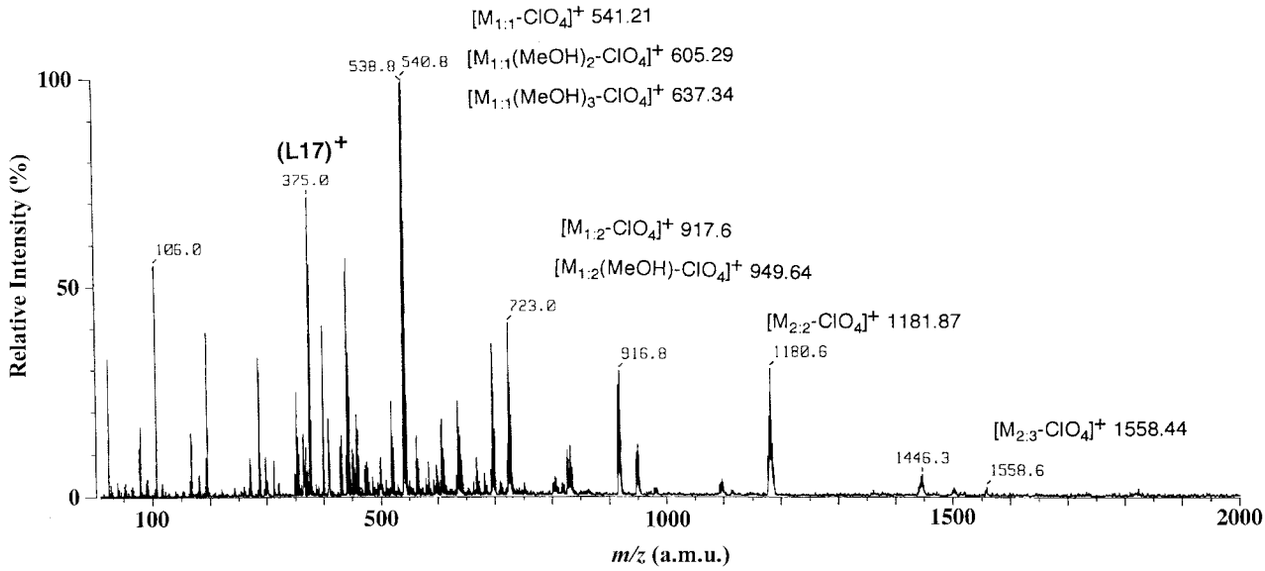

Fig. 4 ESI mass spectrum of a methanol solution of **1**.

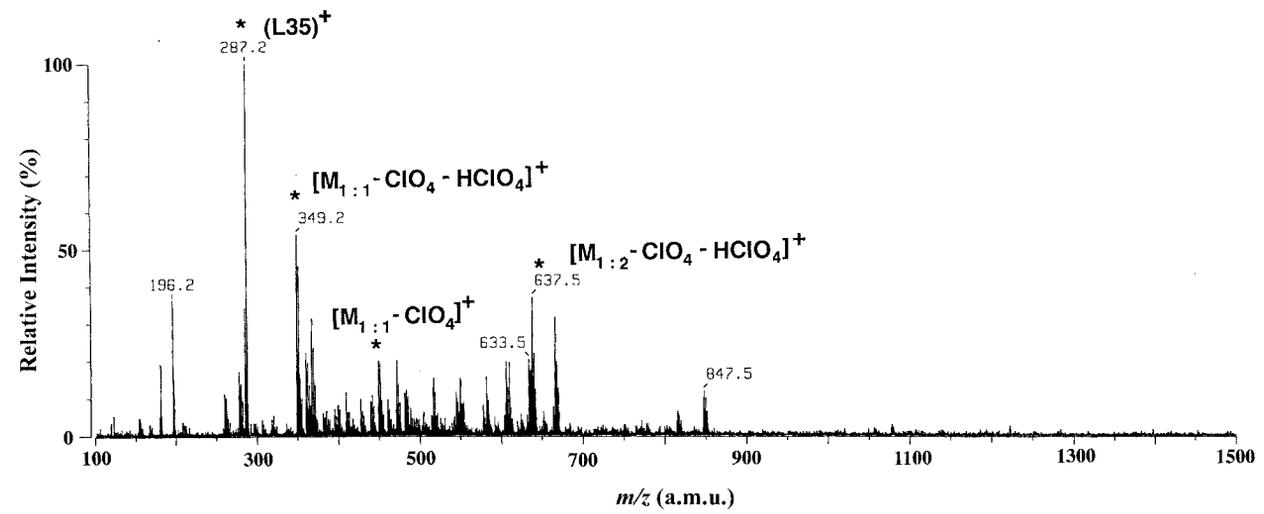

Fig. 5 ESI mass spectrum of a methanol solution of **3**.

X-Ray crystal structure of L^{17}–Zn^{II} complex, 1

Table 1 lists relevant X-ray data for the crystal parameters of **1**. As expected, the formation of a dinuclear structure (Zn^{II}:L^{17} = 2:3) with a triple-helical motif is confirmed as shown in Fig. 6. The complex cation $[(Zn^{II})_2(L^{17})_3]^{4+}$ contains two Zn^{II} ions and three wrapped ligands L^{17}. Selected bond lengths and angles for **1** are presented in Table 2.

The Zn^{II} ions (Zn(1) and Zn(2)) are six-coordinated, being bound by three pyridine nitrogens (py) and three azomethine nitrogens (CH=N) from three L^{17} ligands (L^{17}(1)/C(1)–C(25), N(1)–N(4), L^{17}(2)/C(26)–C(50), N(5)–N(8) and L^{17}(3)/C(51)–C(75), N(9)–N(12)). The lengths of the Zn–N(py) bonds [2.154(6)–2.186(7) Å] are somewhat shorter than those of Zn–N(CH=N) [2.176(6)–2.195 Å]. A slight *trans* influence is observed in the longer Zn(1)–N(5) (2.186(7) Å) and shorter Zn(1)–N(10) (2.176(6) Å). A pseudo-octahedral geometry around Zn(1) is given as judged by the N–Zn–N bond angles N(py)–Zn(1)–N(py), N(py)–Zn(1)–N(CH=N) and N(CH=N)–Zn(1)–N(CH=N). The coordination geometry around Zn(2) is almost the same as that of Zn(1). The interatomic Zn(1)···Zn(2) separation is found to be 11.431 Å. Interestingly, a chiral cavity, which could accommodate small ions such as halide ion, is observed between the three spacer groups. The ClO_4^- ions are too large to be included at the center of the cavity.

The Corey–Pauling–Koltun (CPK) model for $[(Zn^{II})_2(L^{17})_3]^{4+}$ shown in Fig. 7 illustrates the multiple π–π and CH–π aromatic interactions, which operate particularly in some interactive moieties between pyridine–spacer groups (2.8–3.4 Å) and spacer–spacer groups (2.9–3.1 Å), and which create the dinuclear triple-helical structure. The flexibility around the methine group of the spacer (-$C_6H_4CH_2C_6H_4$-) may allow suitable rotational motion of the aromatic rings and CH–π interactions, thereby tuning the triple-helical structure of **1**.

X-Ray crystal structure of L^{16}–Zn^{II} complex, 2

The X-ray crystal structure of $[(Zn^{II})_2(L^{16})_2]\cdot 2CHCl_3$ (**2**·2$CHCl_3$) shows clearly the dinuclear double-helical structure for the neutral complex **2** (Fig. 8). Two Zn^{II} ions (Zn(1) and Zn(2)) and two L^{16} ligand molecules (L^{16}(1)/C(1)–C(27), N(1), N(3), O(1) and O(3) and L^{16}(2)/C(28)–C(54), N(2), N(4), O(2) and O(4)) which are wrapped around the Zn–Zn axis are involved in this supramolecular motif. Table 3 shows the selected bond lengths and angles for **2**.

The Zn^{II} ions are four-coordinated with two phenolate oxygens and two azomethine nitrogens. The two Zn–O bonds are similar (1.895(6) and 1.907(6) Å) and the Zn–N (azomethine) bond 2.019(6)–2.030(6) Å appreciably shorter than the corresponding one in the L^{17}–Zn^{II} complex (2.174(6)–2.247(6) Å). The coordination environment is pseudo-tetrahedral as judged by the N–Zn–N, O–Zn–O and N–Zn–O bond angles. The Zn(1)···Zn(2) separation (11.725 Å) is longer than that of the L^{17}–Zn^{II} complex (11.431 Å).

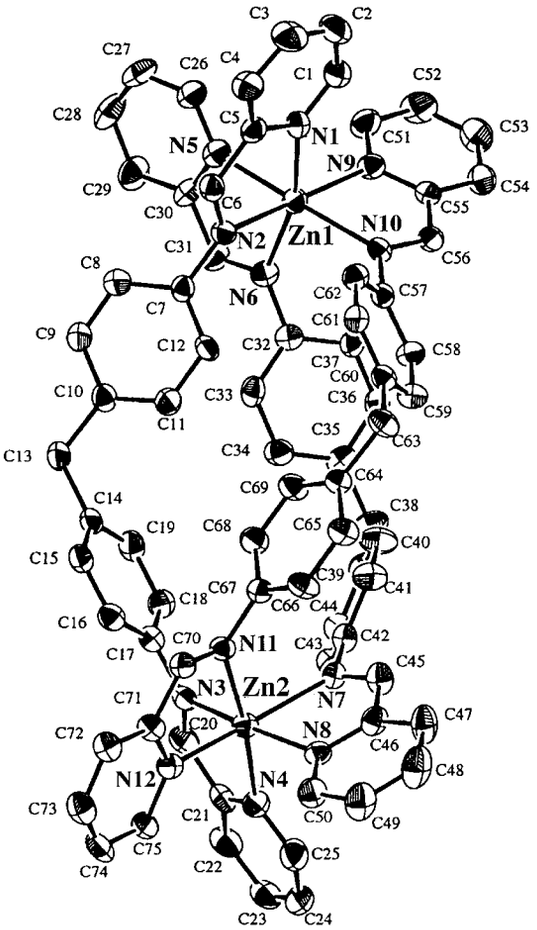

Fig. 6 X-ray crystal structure for **1**. Perchlorate ions are omitted for clarity.

The aromatic rings in the spacer groups are almost parallel to each other (dihedral angle 19.6–21.9°). Effective π–π stacking is observed between these aromatic rings (3.4–3.9 Å). The flexible methine group of the spacer group (-$C_6H_4CH_2C_6H_4$-) and the phenolate coordinating group would lead to the double-helical motif. It is noted that two $CHCl_3$ molecules per complex are trapped within the right-hand cleft. These solvent molecules are held by weak C(H)···Cl hydrogen bonds (3.3–3.9 Å). In the crystal lattice, the left-hand side of aromatic rings of the complex are efficiently stacked with those of another complex molecule.

X-Ray crystal structure of L^{35}–Zn^{II} complex, 3

Recrystallization from DMF–diethyl ether afforded orange blocks of **3**·3DMF. The X-ray crystal structure (Fig. 9 and Table 4) of **3** shows a one-dimensional polynuclear structure as $[Zn^{II}L^{35}(DMF)_2]_n\cdot(DMF)_n\cdot(ClO_4)_{2n}$. The short spacer group (-C_6H_4-) of L^{35} prevents the structure from wrapping around the Zn^{II} ions as observed in L^{17}–Zn^{II} and L^{16}–Zn^{II}. Each zinc ion is six-coordinated with four nitrogens from two L^{35} molecules. Two remaining coordination sites are occupied by two O-bound DMF molecules. Their Zn–O(DMF) bonds are 2.082 and 2.045 Å, respectively. It is noted that few DMF complexes with first-row transition metals have been crystallographically characterized, as pointed out by Ward *et al.*[30] The Zn–N(CH=N) [Zn(1)–N(2) 2.267 and Zn(1)–N(4) 2.238 Å] are appreciably longer than the Zn–N(py) bonds [Zn(1)–N(1) 2.143 and Zn(1)–N(3) 2.141 Å]. The coordination geometry at each Zn^{II} center is pseudo-octahedral with bond angle in the range of O–Zn–O 92.5°, O–Zn–N 87.5–166.9° and N–Zn–N 76.5–161.5°.

Chirality in packing mode

In the solid state of the L^{17}–Zn^{II} complex, it is noted that the

Table 2 Selected bond lengths (Å) and angles (°) for $[(Zn^{II})_2(L^{17})_3](ClO_4)_4$ (**1**) with esds in parentheses

Zn(1)–N(1)	2.158(6)	Zn(1)–N(2)	2.195(5)
Zn(1)–N(5)	2.186(7)	Zn(1)–N(6)	2.193(6)
Zn(1)–N(9)	2.154(6)	Zn(1)–N(10)	2.176(6)
Zn(2)–N(3)	2.174(6)	Zn(2)–N(4)	2.132(7)
Zn(2)–N(7)	2.247(6)	Zn(2)–N(8)	2.167(6)
Zn(2)–N(11)	2.200(6)	Zn(2)–N(12)	2.187(6)
C(6)–N(2)	1.290(9)	C(20)–N(3)	1.264(9)
C(31)–N(6)	1.265(9)	C(45)–N(7)	1.270(9)
C(56)–N(10)	1.268(8)	C(70)–N(11)	1.277(8)
N(1)–Zn(1)–N(2)	76.7(2)	N(1)–Zn(1)–N(5)	91.3(3)
N(1)–Zn(1)–N(6)	164.7(2)	N(1)–Zn(1)–N(9)	98.4(2)
N(1)–Zn(1)–N(10)	94.5(2)	N(2)–Zn(1)–N(5)	87.6(2)
N(2)–Zn(1)–N(6)	93.5(2)	N(2)–Zn(1)–N(9)	173.6(2)
N(2)–Zn(1)–N(10)	99.9(2)	N(5)–Zn(1)–N(6)	76.5(2)
N(5)–Zn(1)–N(9)	96.7(2)	N(5)–Zn(1)–N(10)	171.4(2)
N(6)–Zn(1)–N(9)	92.1(2)	N(6)–Zn(1)–N(10)	98.7(2)
N(9)–Zn(1)–N(10)	76.2(2)		
N(3)–Zn(2)–N(4)	77.3(3)	N(3)–Zn(2)–N(7)	96.0(2)
N(3)–Zn(2)–N(8)	170.1(2)	N(3)–Zn(2)–N(11)	100.6(2)
N(3)–Zn(2)–N(12)	97.9(2)	N(4)–Zn(2)–N(7)	93.2(2)
N(4)–Zn(2)–N(8)	97.1(3)	N(4)–Zn(2)–N(11)	173.3(2)
N(4)–Zn(2)–N(12)	98.4(2)	N(7)–Zn(2)–N(8)	76.1(2)
N(7)–Zn(2)–N(11)	93.4(2)	N(7)–Zn(2)–N(12)	163.6(2)
N(8)–Zn(2)–N(11)	85.8(2)	N(8)–Zn(2)–N(12)	90.9(2)
N(11)–Zn(2)–N(12)	75.4(2)		
Zn(1)–N(1)–C(1)	128.6(5)	Zn(1)–N(1)–C(5)	114.5(5)
Zn(1)–N(2)–C(6)	111.3(5)	Zn(1)–N(2)–C(7)	127.6(5)
Zn(1)–N(5)–C(26)	130.0(6)	Zn(1)–N(5)–C(30)	112.7(5)
Zn(1)–N(6)–C(31)	113.2(5)	Zn(1)–N(6)–C(32)	129.3(5)
Zn(1)–N(9)–C(51)	126.2(6)	Zn(1)–N(9)–C(55)	114.3(4)
Zn(1)–N(10)–C(56)	114.2(4)	Zn(1)–N(10)–C(57)	127.4(4)
Zn(2)–N(3)–C(17)	127.5(5)	Zn(2)–N(3)–C(20)	112.6(6)
Zn(2)–N(4)–C(21)	114.1(6)	Zn(2)–N(4)–C(25)	128.4(6)
Zn(2)–N(7)–C(42)	130.3(5)	Zn(2)–N(7)–C(45)	111.9(5)
Zn(2)–N(8)–C(46)	114.4(4)	Zn(2)–N(8)–C(50)	128.2(6)
Zn(2)–N(11)–C(67)	125.0(4)	Zn(2)–N(11)–C(70)	114.0(5)
Zn(2)–N(12)–C(71)	114.3(5)	Zn(2)–N(12)–C(75)	127.5(5)
C(10)–C(13)–C(14)	114.7(7)	C(35)–C(38)–C(39)	114.5(7)
C(60)–C(63)–C(64)	114.7(6)		

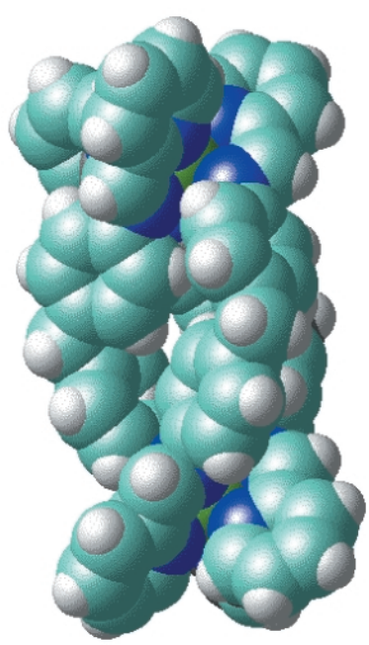

Fig. 7 Space-filling representation of **1**. Perchlorate ions are omitted for clarity.

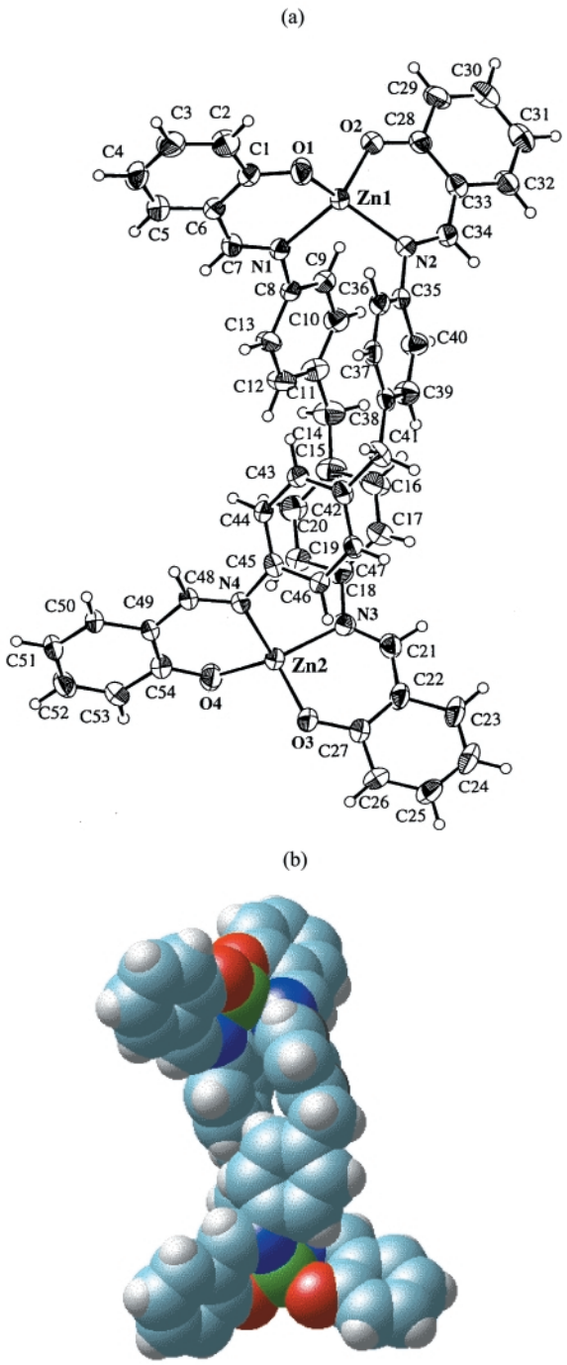

Fig. 8 X-ray crystal structure for **2** (a) and space-filling representation of **2** (b).

ClO_4^- distribution around the complex cation is unsymmetrical. Three counter ClO_4^- ions are located at the periphery of $[(Zn^{II})_2(L^{17})_3]^{4+}$ cation [Zn(1)···ClO_4^- (6.307 and 6.800 Å) and Zn(2)···ClO_4^- (7.579 Å)] while one ClO_4^- ion is situated far from the complex cation to fill the lattice space [Zn(1)···ClO_4^- and Zn(2)···ClO_4^- (12.814 and 12.365 Å)]. In addition, two acetonitrile molecules and one DMF molecule are placed in the pocket formed by the wrapped conformation of three L^{17} ligands.

The $[(Zn^{II})_2(L^{17})_3]^{4+}$ cations have Δ–Δ or Λ–Λ configuration with the Zn^{II} ions. A view from the *a*–*c* plane in the crystal packing of **1** is presented in Fig. 10(a). The Δ–Δ and Λ–Λ optical isomers of **1** are alternately arrayed in the *a*–*c* plane. Four Zn^{II} ions from two $[(Zn^{II})_2(L^{17})_3]^{4+}$ cations along the *a*-axis are situated in the same plane and form a rhombic arrangement with the sum of interior angles 360° (11.431 × 14.459 Å, 47.3 and 132.7°). The other interesting projection of the crystal

Table 3 Selected bond lengths (Å) and angles (°) for $[(Zn^{II})_2(L^{16})_2]$ (**2**) with esds in parentheses

Zn(1)–O(1)	1.895(6)	Zn(1)–O(2)	1.907(6)
Zn(1)–N(1)	2.019(6)	Zn(1)–N(2)	2.030(6)
Zn(2)–O(3)	1.895(5)	Zn(2)–O(4)	1.894(6)
Zn(2)–N(3)	2.020(6)	Zn(2)–N(4)	2.019(7)
O(1)–C(1)	1.328(10)	O(2)–C(28)	1.32(1)
O(3)–C(27)	1.322(9)	O(4)–C(54)	1.340(10)
N(1)–C(7)	1.310(10)	N(2)–C(34)	1.297(10)
N(3)–C(21)	1.30(1)	N(4)–C(48)	1.298(9)
O(1)–Zn(1)–O(2)	111.0(3)	O(1)–Zn(1)–N(1)	95.5(2)
O(1)–Zn(1)–N(2)	129.1(3)	O(2)–Zn(1)–N(1)	126.8(3)
O(2)–Zn(1)–N(2)	95.0(2)	N(1)–Zn(1)–N(2)	102.9(2)
O(3)–Zn(2)–O(4)	112.6(3)	O(3)–Zn(2)–N(3)	96.0(2)
O(3)–Zn(2)–N(4)	119.3(3)	O(4)–Zn(2)–N(3)	129.9(3)
O(4)–Zn(2)–N(4)	96.3(2)	N(3)–Zn(2)–N(4)	104.5(2)
Zn(1)–O(1)–C(1)	126.1(6)	Zn(1)–O(2)–C(28)	127.6(5)
Zn(2)–O(3)–C(27)	126.6(5)	Zn(2)–O(4)–C(54)	122.5(6)
Zn(1)–N(1)–C(7)	119.3(5)	Zn(1)–N(1)–C(3)	120.8(5)
C(7)–N(1)–C(8)	119.7(6)	Zn(1)–N(2)–C(34)	121.3(5)
Zn(1)–N(2)–C(35)	117.9(5)	C(34)–N(2)–C(35)	119.1(6)
Zn(2)–N(3)–C(18)	118.2(5)	Zn(2)–N(3)–C(21)	120.4(5)
C(18)–N(3)–C(21)	120.5(7)	Zn(2)–N(4)–C(45)	120.3(5)
Zn(2)–N(4)–C(48)	119.2(6)		
C(11)–C(14)–C(15)	116.2(7)	C(38)–C(41)–C(42)	115.2(6)

Table 4 Selected bond lengths (Å) and angles (°) for $[Zn^{II}L^{35}]\cdot(ClO_4)_2\cdot$**3**DMF (**3**·3DMF) with esds in parentheses

Zn(1)–O(1)	2.082(3)	Zn(1)–O(2)	2.045(4)
Zn(1)–N(1)	2.143(5)	Zn(1)–N(2)	2.267(4)
Zn(1)–N(3)	2.141(5)	Zn(1)–N(4)	2.238(4)
N(2)–C(6)	1.276(7)	N(4)–C(18)	1.274(7)
O(1)–Zn(1)–O(2)	92.5(1)	O(1)–Zn(1)–N(1)	92.2(2)
O(1)–Zn(1)–N(2)	164.7(2)	O(1)–Zn(1)–N(3)	100.7(1)
O(1)–Zn(1)–N(4)	87.5(1)	O(1)–Zn(1)–N(1)	102.2(2)
O(2)–Zn(1)–N(2)	98.6(1)	O(2)–Zn(1)–N(3)	90.6(2)
O(2)–Zn(1)–N(4)	166.9(2)	N(1)–Zn(1)–N(2)	75.2(2)
N(1)–Zn(1)–N(3)	161.5(1)	N(1)–Zn(1)–N(4)	90.9(2)
N(2)–Zn(1)–N(3)	89.8(2)	N(2)–Zn(1)–N(4)	84.1(1)
N(3)–Zn(1)–N(4)	76.5(2)		
Zn(1)–O(1)–C(19)	124.7(3)	Zn(1)–O(2)–C(22)	128.6(4)
Zn(1)–N(1)–C(1)	125.9(3)	Zn(1)–N(1)–C(5)	115.3(4)
Zn(1)–N(1)–C(5)	115.3(4)	Zn(1)–N(2)–C(6)	110.6(3)
Zn(1)–N(2)–C(7)	125.9(3)	C(6)–N(2)–C(13)	120.9(4)
Zn(1)–N(3)–C(13)	126.9(4)	Zn(1)–N(3)–C(17)	114.9(4)
Zn(1)–N(4)–C(10*)	128.2(3)	Zn(1)–N(4)–C(18)	111.5(3)

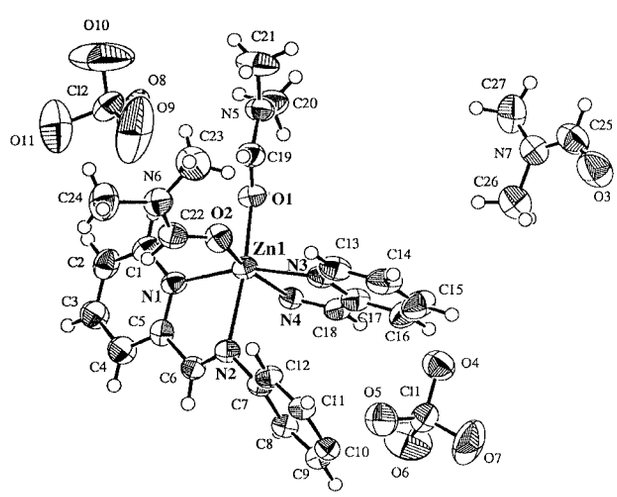

Fig. 9 X-ray crystal structure for **3**·3DMF.

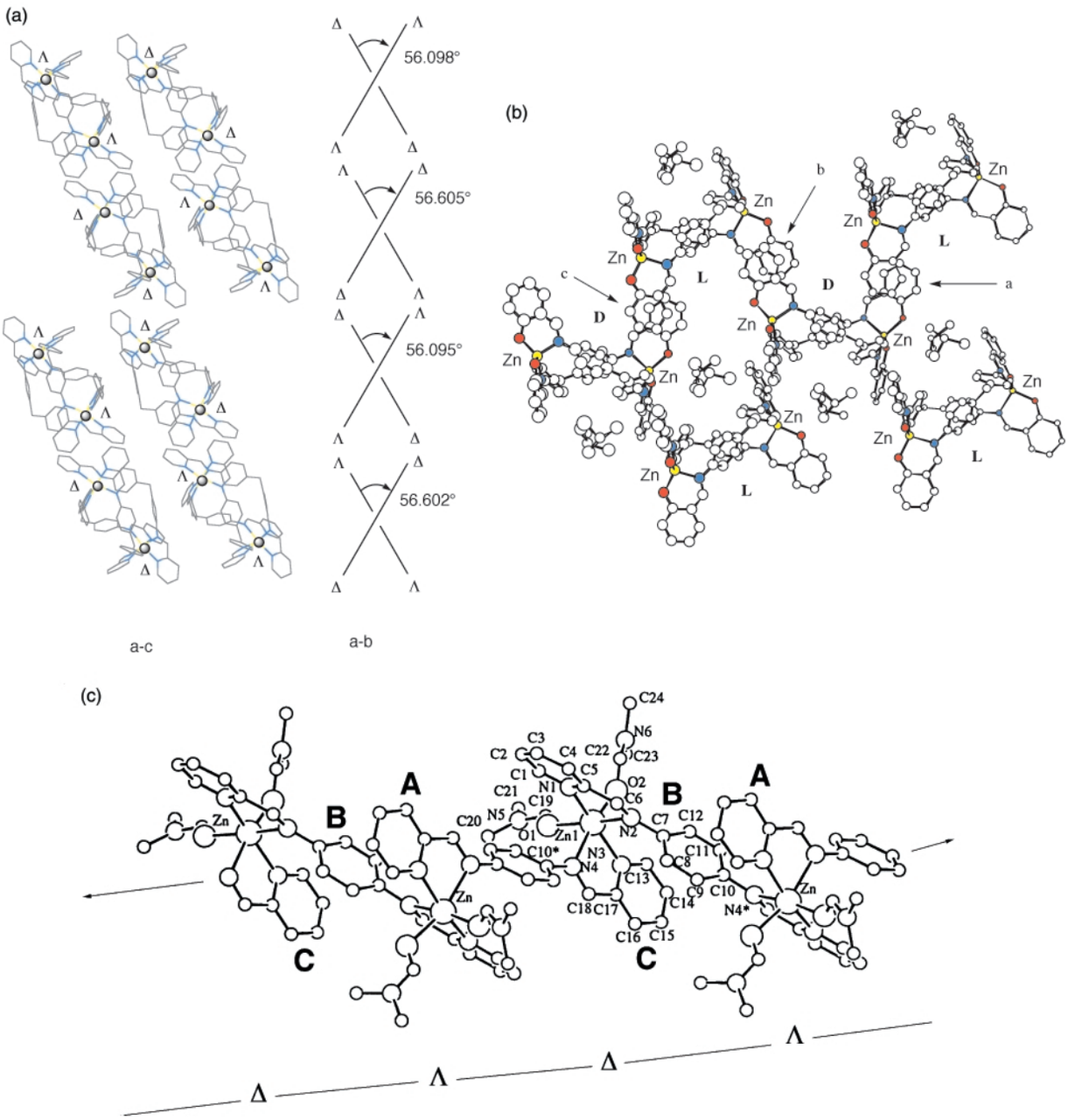

Fig. 10 Chiral packing mode in the solid state of **1** (a), **2** (b) and **3** (c).

packing diagram in the *a*–*b* plane is two intersected Δ–Δ or Λ–Λ isomers with the bite angle 56.6°.

A projection of the crystal packing of **2** in the *b*–*c* plane is presented in Fig. 10(b). Two layers, right-hand (D) and left-hand (L) helicates of the neutral complex **2** are observed in this plane. Sections of the aromatic rings depicted at **a**, **b** and **c** (dihedral angle 2°) have a face-to-face arrangement resulting in infinite π-stacking interactions (roughly the *c* axis in Fig. 10(b)) between adjacent D and L optical isomers of **2**.

A polynuclear zigzag arrangement is observed in the crystal packing of **3** (Fig. 10(c)). In this arrangement, 1D chain with strong-conjugated π-system is formed in the alternating –Δ–Λ–Δ–Λ–Δ– chains. The Zn · · · Zn separation is 9.033 Å. Furthermore, duplicated π-stacking from overlap of aromatic rings in interligand py(A)-spacer(B)-py(C) sites are observed.

Solution structure of L^{17}–Zn^{II} and L^{16}–Zn^{II} complexes

The crystal structure of complex **1** shows the formation of dinuclear triple-helical $[(Zn^{II})_2(L^{17})_3]^{4+}$ species, while ESI mass spectrum indicates the mixture of some aggregated species such as $(Zn^{II}:L^{17})^{n+} = (1:1)^+$, $(1:2)^+$, $(2:2)^+$, and $(2:3)^+$ species. If the L^{17}–Zn^{II} complex is to retain a $(2:3)^+$ structure in solution, the ^{1}H NMR spectrum should exhibit one set of sharp signals. The ^{1}H NMR spectra in DMF-d_7 of complex **1** and a comparison with its ligand L^{17} are shown in Fig. 11.

The room temperature spectrum of **1** indicates peak broadening in all protons. This broadening may arise from instability of the complex or exchange on the NMR time scale between different species including ligand molecule. Sharper signals are obtained at − 20 °C. Since the exchange is fast on the ^{1}H NMR time scale, we cannot determine precisely from these spectra alone the extent of ligand dissociation by integrating peaks associated with the zinc-bound and dissociated L^{17} ligand. In general, the protons of H(1) and H(2) of the py moiety tend to shift downfield (H(1)* and H(2)*) upon complexation. In particular, the azomethine proton H(5) shows much a larger downfield shift due to the -CH(5)=N- coordination to Zn^{II} ion. However, two sets of spacer group resonances at H(6)* and H(7)* show large upfield shifts. These pronounced upfield shifts may be attributed to the CH · · · π interaction between the spacer aromatic protons and py moiety,

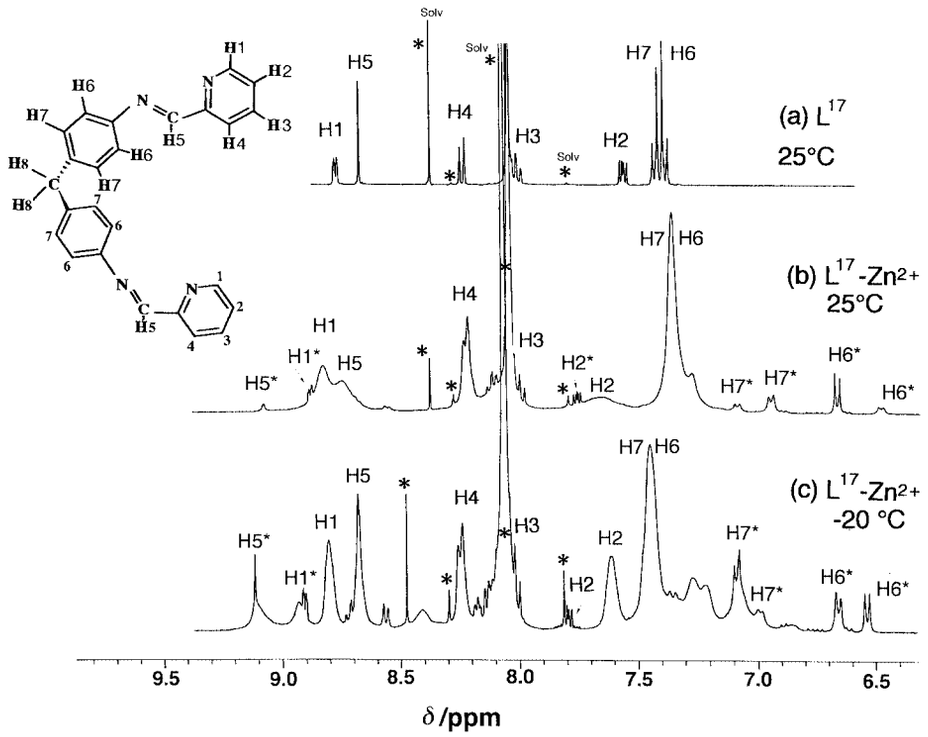

Fig. 11 ^{1}H NMR spectra of L^{17} and its Zn^{II} complex $[(Zn^{II})_2(L^{17})_3](ClO_4)_4$, **1**.

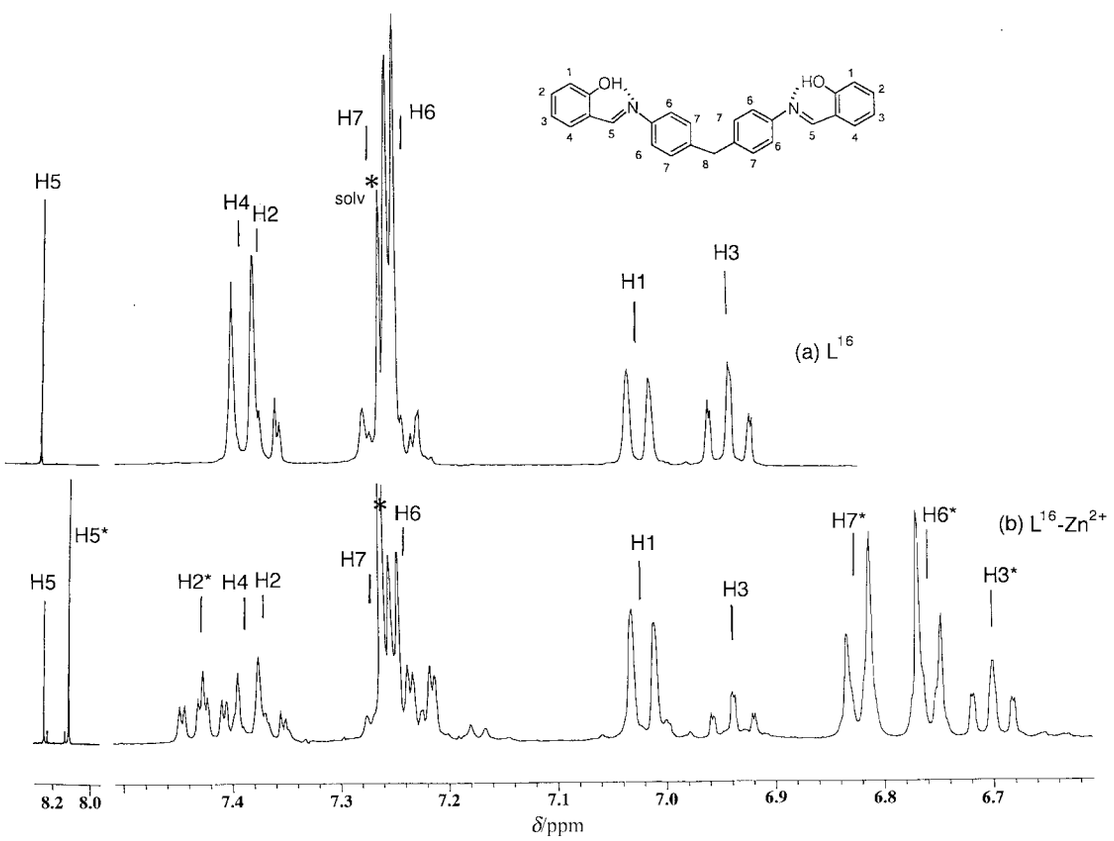

Fig. 12 ^{1}H NMR spectra of L^{16} and its Zn^{II} complex $[(Zn^{II})_2(L^{16})_2]$, **2**.

which is mentioned for the $[(Zn^{II})_2(L^{17})_3]^{4+}$ complex in the solid-state.

In contrast to complex **1**, the ^{1}H NMR spectrum of **2** in $CDCl_3$ at 25 °C is simple to interprete and sharply resolved into the ligand peak and complex peak (Fig. 12). The integrating ratio of peak is about 1 : 2 (ligand : complex). Upon complexation of L^{16} with Zn^{II} ion, large upfield shift, due to the deprotonation of the phenolic group, is observed particularly in the protons of H(3) and H(5). The large upfield shift observed in the protons of spacer group (H(6)→H(6)* and H(7)→H(7)*) of **2** would be ascribed to the existence of CH · · · π interactions in solution.

Conclusion

The series of Zn^{II} complexes with L^{16}, L^{17} and L^{35} have been found to show interesting variations of structure in the solid-

state and solution. Three Zn^{II}-assisted supramolecular motifs were presented using the bis-bidentate Schiff bases L^{16}, L^{17} and L^{35}, having flexible aromatic spacer groups. X-Ray crystal diffraction characterization revealed that the L^{16}–Zn^{II}, L^{17}–Zn^{II} and L^{35}–Zn^{II} complexes display dinuclear double-helical, dinuclear triple-helical and 1-D polynuclear architectures in the solid-state, depending on subtle differences of coordination site and spacer group in the ligand. UV/VIS, ESI-MS and ^{1}H NMR data were also consistent with the formation of these species in solution. The coordinatively flexible Zn^{II} ion and the aromatic–aromatic interactions between the flexible spacer group in the wrapped ligands would be a crucial factor for the formation of the supramolecular structure. Three types of chiral-linking mode have been generated for the crystal packing in the L^{16}–Zn^{II}, L^{17}–Zn^{II} and L^{35}–Zn^{II} complexes.

References

1 Part 4. N. Yoshida, H. Oshio and T. Ito, *J. Chem. Soc.*, *Perkin Trans. 2*, 1999, 975.
2 N. Yoshida and K. Ichikawa, *Chem. Commun.*, 1997, 1091; N. Yoshida, H. Oshio and T. Ito, *Chem. Commun.*, 1998, 63.
3 N. Yoshida, N. Ito and K. Ichikawa, *J. Chem. Soc.*, *Perkin Trans. 2*, 1997, 2387.
4 M. J. Hannon, C. L. Painting and N. W. Alcock, *Chem. Commun.*, 1999, 2023; L. Douce, A. El-ghayoury, A. Skoulios and R. Ziessel, *Chem. Commun.*, 1999, 2033; S. Brooker, P. G. Plieger, B. Moubaraki and K. S. Murray, *Angew. Chem.*, *Int. Ed.*, 1999, **38**, 408; M. J. Hannon, S. Bunce, A. J. Clarke and N. W. Alcock, *Angew. Chem.*, *Int. Ed.*, 1999, **38**, 1277; S. Brooker, R. J. Kelly and P. G. Plieger, *Chem. Commun.*, 1998, 1079; P. K. Bowyer, K. A. Porter, A. D. Rae, A. C. Willis and S. B. Wild, *Chem. Commun.*, 1998, 1153; M. J. Hannon, C. L. Painting, A. Jackson, J. Hamblin and W. Errington, *Chem. Commun.*, 1997, 1807; P. Comba, A. Fath, G. Huttner and L. Zsolnai, *Chem. Commun.*, 1996, 1885.
5 B. J. McNeils, L. C. Nathan and C. J. Clark, *J. Chem. Soc.*, *Dalton Trans.*, 1999, 1831; M.-L. Tong, X.-M. Chen, B. H. Ye and L.-N. Ji, *Angew. Chem.*, *Int. Ed.*, 1999, **38**, 2237.
6 C. Bonnefous, N. Bellec and R. P. Thummel, *Chem. Commun.*, 1999, 1243.
7 (*a*) K. L. V. Mann, J. C. Jeffery, J. A. McCleverty, P. Thornton and M. D. Ward, *J. Chem. Soc.*, *Dalton Trans.*, 1998, 89; (*b*) J. C. Jeffery, P. L. Jones, K. L. V. Mann, E. Psillakis, J. A. McCleverty, M. D. Ward and C. M. White, *Chem. Commun.*, 1997, 175.
8 O. Mamula, A. von Zelewsky and G. Bernardinelli, *Angew. Chem.*, *Int. Ed.*, 1998, **37**, 290.
9 R. W. Saalfrank, N. Löw, B. Demleitner, D. Stalke and M. Teichert, *Chem. Eur. J.*, 1998, **4**, 1305.
10 D. C. Caulder, R. E. Powers, T. N. Parac and K. N. Raymond, *Angew. Chem.*, *Int. Ed.*, 1998, **37**, 1840.
11 J. R. Farrell, C. A. Mirkin, I. A. Guzei, L. M. L.-Sands and A. L. Rheingold, *Angew. Chem.*, *Int. Ed.*, 1998, **37**, 465.
12 M. Albrecht, *Chem. Eur.*, 1997, **3**, 1466.
13 V. A. Grillo, E. J. Seddon, C. M. Grant, G. Aromí, J. C. Bollinger, K. Folting and G. Christou, *Chem. Commun.*, 1997, 1561; V. A. Grillo, M. J. Knapp, J. C. Bollinger, D. N. Hendrickson and G. Christou, *Angew. Chem.*, *Int. Ed. Engl.*, 1996, **35**, 1818.
14 U. Velten and M. Rehahn, *Chem. Commun.*, 1996, 2639.
15 L. J. Charbonniére, M.-F. Gilet, K. Bernauer and A. F. Williams, *Chem. Commun.*, 1996, 39.
16 (*a*) J.-M. Lehn, *Supramolecular Chemistry*, VCH, Weinheim, 1995; (*b*) D. Philp and J. F. Stoddart, *Angew. Chem.*, *Int. Ed. Engl.*, 1996, **35**, 1154.
17 B. Hasenknopf, J.-M. Lehn, N. Boumediene, E. Leize and A. V. Dorsselaer, *Angew. Chem.*, *Int. Ed.*, 1998, **37**, 3265; B. Hasenknopf, J.-M. Lehn, N. Boumediene, A. D.-Gervais, A. V. Dorsselaer and D. Fenske, *J. Am. Chem. Soc.*, 1997, **119**, 10956; B. Hasenknopf, J.-M. Lehn, B. O. Kneisel, G. Baum and D. Fenske, *Angew. Chem.*, *Int. Ed. Engl.*, 1996, **35**, 1838.
18 R. Vilar, D. M. P. Mingos, A. J. P. White and D. J. Williams, *Chem. Commun.*, 1999, 229; J. S. Fleming, K. L. V. Mann, C.-A. Carraz, E. Psillakis, J. C. Jeffery, J. A. McCleverty and M. D. Ward, *Angew. Chem.*, *Int. Ed.*, 1998, **37**, 1279; D. A. McMorran and P. J. Steel, *Angew. Chem.*, *Int. Ed.*, 1998, **37**, 3295; P. L. Jones, J. C. Jeffery, J. A. McCleverty and M. D. Ward, *Chem. Commun.*, 1997, 1361.
19 R.-D. Schnebeck, E. Freisinger and B. Lippert, *Angew. Chem., Int. Ed.*, 1999, **38**, 168; S. Mann, G. Huttner, L. Zsolnai and K. Heinze, *Angew. Chem.*, *Int. Ed. Engl.*, 1996, **35**, 2808.
20 M. Albrecht, O. Blau and R. Fröhlich, *Chem. Eur. J.*, 1999, **5**, 48; M. Albrecht, H. Röttele and P. Burger, *Chem. Eur. J.*, 1996, **2**, 1264.
21 M. Tadokoro, K. Isobe, H. Uekusa, Y. Ohashi, J. Toyoda, K. Tashiro and K. Nakasuji, *Angew. Chem., Int. Ed.*, 1999, **38**, 95; H. Miyasaka, S. Okamura, T. Nkashima and N. Matsumoto, *Inorg. Chem.*, 1997, **36**, 4329.
22 A. Marquis-Rigault, A. Dupont-Gervas, A. V. Dorsselaer and J.-M. Lehn, *Chem. Eur. J.*, 1996, **2**, 1395; C. R. Woods, M. Benaglia, F. Cozzi and J. S. Siegel, *Angew. Chem.*, *Int. Ed. Engl.*, 1996, **35**, 1830.
23 D. C. Rees, M. Lewis and W. N. Lipscomb, *J. Mol. Biol.*, 1983, **168**, 367; D. R. Holland, A. C. Haustrath, D. Juers and B. W. Matthews, *Protein Sci.*, 1995, **4**, 1955.
24 S. K. Nair and D. W. Christianso, *J. Am. Chem. Soc.*, 1991, **113**, 9455; D. N. Silverman and S. Lindskog, *Acc. Chem. Res.*, 1988, **21**, 30.
25 E. E. Kim and H. W. Wyckoff, *J. Mol. Biol.*, 1991, **218**, 449.
26 M. Nishio, M. Hirota and Y. Umezawa, *The CH/π Interaction-Evidence, Nature and Consequences*, Wiley-VCH, New York, 1998.
27 SIR92: A. Altomare, M. C. Burla, M. Camalli, M. Cascarano, C. Giacovazzo, A. Guagliardi and G. Polidori, *J. Appl. Crystallogr.*, **27**, 435 (1994).
28 DIRDIF94 (1994): P. T. Beurskens, G. Admiraal, G. Beurskens, W. P. Bosman, R. de Gelder, R. Israel and J. M. M. Smiths, The DIRDIF-94 program system, Technical Report of the Crystallography Laboratory, University of Nijmegen, The Netherlands.
29 teXsan: Crystal Structure Analysis Package, Molecular Structure Corporation (1985 and 1992).
30 D. A. Bardwell, J. C. Jeffery and M. D. Ward, *J. Chem. Soc. Dalton Trans.*, 1995, 3071.

Paper a908041d